GUIDANCE DOCUMENT

Geo-location Requirements for UXO Discrimination

ESTCP Project MM-0413

May 2008

Thomas Bell
SAIC

Environmental Security Technology
Certification Program

Report Documentation Page

Form Approved
OMB No. 0704-0188

1. REPORT DATE	2. REPORT TYPE	3. DATES COVERED
01 MAY 2008	**N/A**	**-**

4. TITLE AND SUBTITLE	5a. CONTRACT NUMBER
Geo-location Requirements for UXO Discrimination (Guidance Document)	5b. GRANT NUMBER
	5c. PROGRAM ELEMENT NUMBER
6. AUTHOR(S) **Dr. Thomas H. Bell**	5d. PROJECT NUMBER **MM-0413**
	5e. TASK NUMBER
	5f. WORK UNIT NUMBER
7. PERFORMING ORGANIZATION NAME(S) AND ADDRESS(ES) **SAIC 1225 South Clarke Street, Suite 800 Arlington, VA 22202**	8. PERFORMING ORGANIZATION REPORT NUMBER
9. SPONSORING/MONITORING AGENCY NAME(S) AND ADDRESS(ES) **Environmental Security Technology Certification Program 901 North Stuart Street, Suite 303 Arlington, VA 22203**	10. SPONSOR/MONITOR'S ACRONYM(S) **ESTCP**
	11. SPONSOR/MONITOR'S REPORT NUMBER(S)

12. DISTRIBUTION/AVAILABILITY STATEMENT
Approved for public release, distribution unlimited

13. SUPPLEMENTARY NOTES
The original document contains color images.

14. ABSTRACT

15. SUBJECT TERMS

16. SECURITY CLASSIFICATION OF:			17. LIMITATION OF ABSTRACT	18. NUMBER OF PAGES	19a. NAME OF RESPONSIBLE PERSON
a. REPORT **unclassified**	b. ABSTRACT **unclassified**	c. THIS PAGE **unclassified**	**UU**	**22**	

Contents

Figures

Acronyms

APG	Aberdeen Proving Ground
DGM	Digital Geophysical Mapping
DMM	Discarded Military Munitions
EMI	Electromagnetic Induction
ESTCP	Environmental Security Technology Certification Program
GPS	Global Positioning System
MEC	Munitions and Explosives of Concern
MTADS	Multisensor Towed Array Detection System
RMS	Root Mean Square
RTK	Real Time Kinematic
SERDP	Strategic Environmental Research and Development Program
SNR	Signal to Noise Ratio
UXO	Unexploded Ordnance
YPG	Yuma Proving Ground

1. Introduction

The Environmental Security Technology Certification Program (ESTCP) sponsored the development and operation of Standardized Test Sites at Aberdeen Proving Ground (APG), Maryland, and Yuma Proving Ground (YPG), Arizona. The purpose of these sites is to provide a means for characterizing the performance of technologies under development for the detection and discrimination of Munitions and Explosives of Concern (MEC), which include Unexploded Ordnance (UXO) and Discarded Military Munitions (DMM) [1]. ESTCP Project MM-0413 implemented standardized, data-level evaluations of demonstration performance at the Standardized UXO Test Sites in order to support an understanding of the capabilities and limitations of the various UXO detection and discrimination sensors [2]. Generally speaking the conclusions drawn by MM-0413 were disappointing. Only a relatively small fraction of the survey data analyzed for that project was accurate enough to support reliable feature-based target classification and discrimination. Even when the target Signal to Noise Ratio (SNR) was relatively high the quality of the estimated target parameters was frequently relatively poor. This suggests that the problems are due to deficiencies in the surveys, *e.g.* sensor location errors. This report presents the results on an analysis of the effects of sensor location errors (geo-location errors) on target classification and discrimination performance, and provides guidance on the geo-location accuracy requirements for reliable target classification.

Buried UXO are found with metal detectors. There are two kinds of metal detectors: magnetometers and electromagnetic induction (EMI) sensors. Magnetometers measure the local magnetic field. Many UXO are made of iron or steel. Being ferromagnetic they distort the earth's magnetic field, and magnetometers can be used to locate the resulting magnetic anomalies. EMI sensors use electromagnetic fields to excite or induce a response from nearby metal objects.

Much of the material in the ground at a UXO cleanup site is clutter, not UXO. All the bits and pieces of metal in the ground that are not UXO are clutter – exploded ordnance fragments, range scrap and agricultural or industrial artifacts such as horseshoes, broken implements, *etc*. Since much of this clutter could safely be left in the ground, cleanup efficiency could be significantly improved were it possible to reliably distinguish or discriminate between buried UXO and clutter in the ground. Magnetometer data can be used to determine the location and depth of a buried object, get a rough idea of its size, and perhaps determine whether or not it has significant remnant magnetization [3, 4]. Although such information can be useful for classification and discrimination [5, 6], EMI sensors provide significantly more information for characterizing buried objects. Specifically, because EMI sensors can excite an object from different directions they can be used to obtain information relating to the shape of the object as well as its size [7-13].

Several projects underway within SERDP/ESTCP and elsewhere are attempting to develop sensor arrays configured in such a way that they can simultaneously excite the target from the full complement of directions. However, with currently available commercial EMI sensors, the only reliable technique for target characterization employs model-based inversion of data collected as the sensor is moved around over the target [9, 10, 12]. The data must be spatially mapped in order for the inversion procedure to isolate the different signal contributions that arise when the target is excited from different directions. Errors in the recorded locations of the sensor readings relative to each other can seriously degrade target characterization and discrimination performance. Absolute errors are not so important. A uniform absolute offset affects only the estimated target location and does not degrade the accuracy of parameter estimates relating to target depth, shape or orientation.

This report summarizes the geo-location requirements for UXO discrimination based on inversion of spatially mapped data. We distinguish between absolute position accuracy needed for target reacquisition and the relative accuracy needed to support data inversion. Section 2 briefly reviews the (absolute) geo-location requirements for buried UXO detection and recovery. Discrimination between UXO and clutter using geophysical data is discussed in Section 3. Concepts and practical considerations of performing inversion on spatially mapped data are explained there. Section 4 covers the (relative) geo-location requirements for reliable inversion of spatially mapped data. We present results on the accuracy of target parameter estimates as functions of the accuracy of measured locations of data points and relate the results to the errors due to other sources of noise. The important conclusions regarding the geo-location requirements for UXO discrimination are summarized in Section 5. We have included selected references (cited at appropriate places in the text) that should serve as a useful entry point to the relevant topics. Much of the material in this report was presented at the SERDP/ESTCP Geo-location Workshop held in Annapolis, MD in June 2005.

2. Geo-location Requirements for Buried UXO Detection and Recovery

There are two basic approaches to locating buried UXO: "mag and flag" and digital geophysical mapping. Historically, "mag and flag" methodology has been the standard approach used to locate buried ordnance. In this approach, UXO technicians walk up and down over the site, sweeping a hand-held metal detector from side to side. Whenever the instrument indicates the presence of a piece of metal, the technician places a small flag in the ground and continues on. Later, a team comes along to excavate and dispose of the UXO. As long as the flags remain in the ground and are not too overgrown, the recovery team knows pretty much where to dig.

Over the last decade, digital geophysical mapping (DGM) has emerged as a superior approach in most situations [14-16]. The advantages of DGM that are usually cited include improved UXO detection, cost savings due to some clutter rejection, and a permanent record of the survey. With DGM, the sensor data are recorded digitally. The spatial locations of the readings are usually either (a) determined from Global Positioning System (GPS) data collected simultaneously with the sensor data or (b) based on interpolation over the tracks using a dead reckoning scheme. Geo-location systems based on ultrasonic positioning and automated laser surveying equipment have also been used.

Figure 1 is an example of DGM. It shows mapped magnetic field data that were collected for ESTCP by the Naval Research Laboratory using the Multisensor Towed Array Detection System (MTADS) [15, 17] at the APG Standardized UXO Test Site Blind Grid. The MTADS array consists of eight total field magnetometers towed behind a low magnetic signature vehicle. The data are geo-located with real time kinematic (RTK) differential GPS using an antenna on the tow platform. The locations of possible buried UXO are determined by fitting a model for the expected magnetic field distortion due to a compact piece of iron or steel to each of the magnetic anomalies in the map. The fitting procedure uses a Levenberg-Marquardt gradient search technique to determine the target parameters (location, depth, magnetic dipole strength and orientation) that minimize the mean squared error between the model and the measured data.

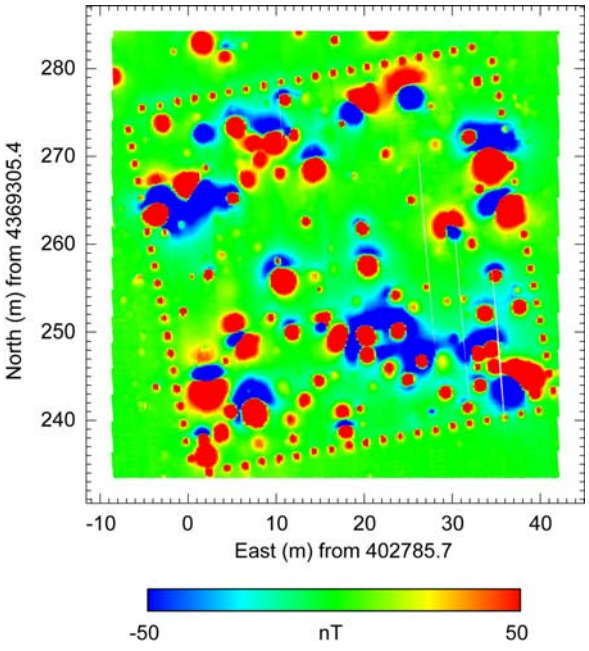

Figure 1 – MTADS magnetometer survey of the Blind Grid at the APG Standardized UXO Test Site.

Efficient excavation and disposal of suspected UXO targets requires that the target locations determined from the mapped data be reasonably accurate. Target location errors for systems demonstrated at the APG and YPG Standardized UXO Test Sites typically averaged from 15 to 35 cm. Figure 2 shows a histogram of average target location errors for the various demonstrators based on the results reported in the Standardized Test Sites Project Final Report [1]. Given the nature of target excavation, the sort of absolute location accuracy portrayed in Figure 2 is perfectly acceptable for purposes of target detection and remediation. Indeed, most of the target locations were determined from the survey data to within a shovel's width and/or the size of the object itself.

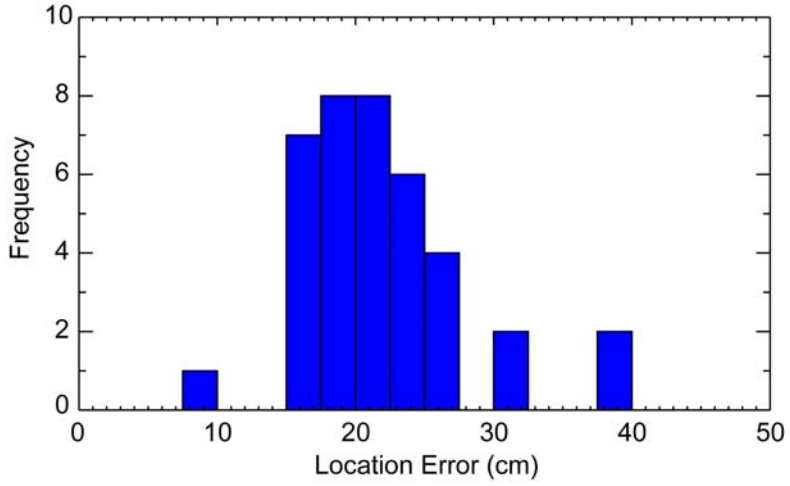

Figure 2 – Histogram of average target location errors for demonstrators at the APG and YPG Standardized UXO Test Sites.

3. Discrimination Between UXO and Clutter

As noted in the introduction, much of the material in the ground at UXO cleanup sites is not UXO, but clutter – exploded ordnance fragments, range scrap and agricultural or industrial artifacts such as horseshoes, broken implements, etc. UXO sensors detect clutter along with buried UXO. In principal, at least some of this clutter could safely be left in the ground. Magnetometer data provides some information that is useful for distinguishing between UXO and clutter. The magnetic signature of a UXO or clutter item has two components: induced magnetization due to the geomagnetic field and remnant magnetization related to the item's history of magnetic exposure. These effects can be modeled quite accurately in terms of a magnetic dipole at the "center" of the object. The strength and orientation of the induced dipole moment are determined by the object's size, shape and orientation relative to the earth's magnetic field [18]. We can invert spatially mapped magnetometer data to determine the location, depth, and magnetic dipole strength and orientation that best characterize the target. The procedure employs a Levenberg-Marquardt gradient search technique to determine the target parameters that minimize the mean squared error between the field due to the dipole and the measured data.

Dipole strength correlates well with UXO size (caliber), which can be exploited to estimate target size from magnetic data collected over the target. Figure 3 compares the calculated target size with the actual size (caliber) for a variety of ordnance items at two UXO test sites. The relationship between calculated or apparent target size α and dipole moment strength M used in Figure 3 is

$$\alpha = (M / B_E)^{1/3} \tag{1}$$

where B_E is the geomagnetic field strength. The RMS spread about the diagonal in Figure 3 is ±28%. This reflects the uncertainty in the size estimate due to variations in the target orientation relative to the geomagnetic field, variations in the target length to diameter aspect ratio, and remnant magnetization. If remnant magnetization is not a significant factor for the UXO, then dipole moment strength and orientation may be compared with expected ranges of values for expected UXO at a site, providing some potential for classifying magnetic anomalies with respect to the likelihood that they are due to UXO rather than clutter [19].

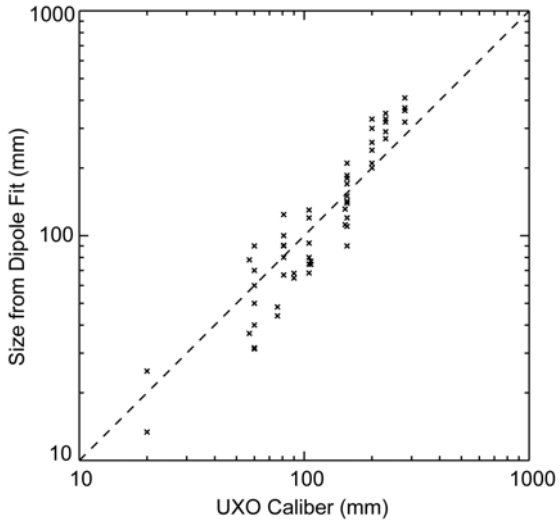

Figure 3 – Target size from magnetic dipole fits to mapped data compared with actual UXO size.

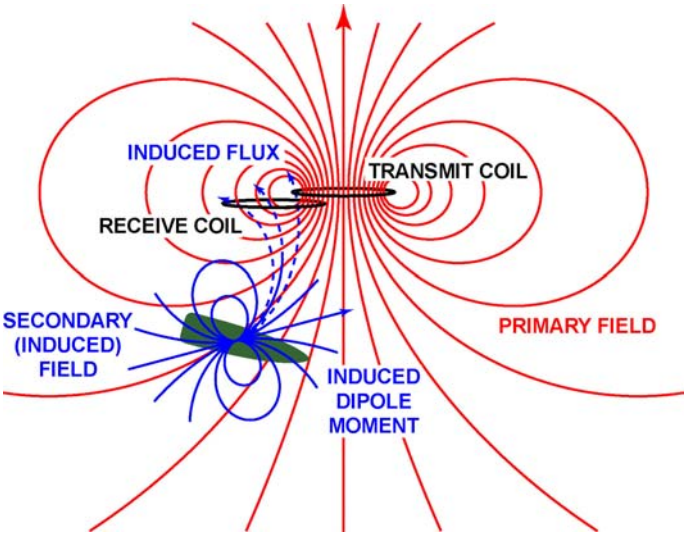

Figure 4 – Basic elements of an EMI sensor.

EMI sensors can provide significantly more information for characterizing buried objects than can magnetometers. Because EMI sensors can excite an object from different directions they can be used to obtain information relating to the shape of the object as well as its size and composition (electrical conductivity and magnetic permeability). These intrinsic properties of the target can be used with statistical decision rules to discriminate between UXO and clutter. Target shape is especially significant because most UXO are long and slender, having been designed to be shot from guns or dropped from aircraft and to maintain a steady trajectory. Clutter items come in an endless variety of shapes. Here, we will address the factors that affect our ability to estimate intrinsic target parameters, especially those relating to target shape, from EMI data collected above the target. Specifically, we will consider the effects of background noise levels and geo-location errors.

The basic operation of an EMI sensor is illustrated schematically in Figure 4. An EMI sensor typically consists of a transmit coil and a receive coil. Current flowing in the transmit coil produces the primary field $\mathbf{H}_0$ shown in red. Changes in the primary field $\mathbf{H}_0$ induce eddy currents in the target, which in turn produce the induced field $\mathbf{H}_I$ shown in blue. The signal S(t) is proportional to the receiver voltage V(t) created by a changing magnetic flux through the receive coil due to $\mathbf{H}_I$. The target response to the primary field can be represented in terms of an induced dipole moment that depends on the strength and orientation of the primary field at the target and on the size, shape, composition and orientation of the target.

To a very good approximation, the target response can be represented in terms of the magnetic polarizability along each of its principal axes. A magnetic polarizability matrix $\mathbf{B}$ describes the induced dipole response of the target [20, 21]. For an ideal time-domain sensor (current maintained at a constant level I_0 and then instantaneously returned to zero), the EMI signal S is represented in terms of $\mathbf{B}$ as

$$S(t) = \mu_0 A I_0 \mathbf{C}_R \cdot \mathbf{C}_T \mathbf{B}(t) . \qquad (2)$$

A completely analogous expression, connected to (2) by Fourier transform relationships, holds for frequency domain sensors. In equation (2) $\mathbf{C}_T$ and $\mathbf{C}_R$ are coil sensitivity functions for the transmit and receive coil, μ_0 is the magnetic permeability of free space ($4\pi x10^{-7}$ volt-sec/amp-m) and A is a scaling factor that depends on the number of turns in the transmit and receive coils, the receiver gain, *etc.* $\mathbf{C}_T$ and

$\mathbf{C}_R$ depend only on coil geometry and location relative to the target, while $\mathbf{B}$ depends only on what the target is, not where it is.

The coil sensitivity functions are vectors that specify (a) the strength and orientation of the primary field at the target ($\mathbf{C}_T$) and (b) the sensitivity of the receive coil to the vector components of a magnetic dipole source at the target location ($\mathbf{C}_R$). The vector $\mathbf{C}_T\mathbf{B}$ describes the strength of the induced target response in the X, Y and Z coordinate directions. Taking the dot product with $\mathbf{C}_R$ accounts for the relative sensitivity of the receive coil to each of these response components.

The strength and orientation of $\mathbf{C}_T$ and $\mathbf{C}_R$ are sensitive functions of the location of the EMI sensor relative to the target. $\mathbf{C}_T$ and $\mathbf{C}_R$ are defined in terms of integrals around the coil involving the vector from the target to the coil:

$$\mathbf{C}_{T,R}(\mathbf{r}_0) = \frac{1}{4\pi} \oint_{T,R} \frac{d\mathbf{l} \times (\mathbf{r}_0 - \mathbf{r})}{|\mathbf{r}_0 - \mathbf{r}|^3} \tag{3}$$

where $\mathbf{r}_0$ is the location of the target and $\mathbf{r}$ is the location of a point on the coil. When all is said and done, it is the sensitivity of $\mathbf{C}_T$ and $\mathbf{C}_R$ to the location of the EMI sensor relative to the target that drives the geo-location problem as it relates to target classification and discrimination. If the sensor is moving while the data are collected, then any dynamic response characteristics of the sensor have to be included in the forward model (2) for the EMI signal. This can be a significant effect of the Geonics EM61 class of sensors which use analog averaging of the signal [22].

As a consequence of electromagnetic reciprocity, the matrix $\mathbf{B}$ is symmetric. By a suitable rotation it can be transformed to diagonal form, so we can write

$$\mathbf{B} = \mathbf{U}\mathbf{B}_0\mathbf{U}^T \tag{4}$$

with

$$\mathbf{B}_0 = \begin{bmatrix} \beta_1 & 0 & 0 \\ 0 & \beta_2 & 0 \\ 0 & 0 & \beta_3 \end{bmatrix}. \tag{5}$$

In terms of yaw, pitch and roll Euler angles θ, ϕ and ψ [23], the rotation matrix $\mathbf{U}$ is given by

$$\mathbf{U} = \begin{bmatrix} \cos\theta\cos\phi & \cos\theta\sin\phi & -\sin\theta \\ \sin\psi\sin\theta\cos\phi - \cos\psi\sin\phi & \sin\psi\sin\theta\sin\phi + \cos\psi\cos\phi & \cos\theta\sin\psi \\ \cos\psi\sin\theta\cos\phi + \sin\psi\sin\phi & \cos\psi\sin\theta\sin\phi - \sin\psi\cos\phi & \cos\theta\cos\psi \end{bmatrix}. \tag{6}$$

The eigenvalues β_1, β_2, β_3 correspond to responses induced by field components aligned with each of the target object's principal axes. θ, ϕ and ψ together define the orientations of these principal axes. In general, the aggregate magnitude of the βs is determined by the size of the object, while differences among the βs are related to the object's shape. Both dependencies are exploited for target classification and discrimination. Depending on sensor modality the βs are functions either of time after the primary field cutoff or of the frequency of the primary field; the Euler angles are not. For UXO-like objects, these

functions tend to have rather simple forms that can be expressed in terms of two or three parameters [10, 24, 25]. Many different objects can have more or less the same response, depending on their orientation and location relative to the sensor. However, they will not respond the same for all orientations. The interrelationship of the βs is what allows us to distinguish between different objects of more or less the same size.

For signatures of UXO items collected using the standard Geonics EM61, we have one large β corresponding to an axially excited dipole and two smaller, equal βs corresponding to transverse excitation, perpendicular to the long axis of the UXO item. Figure 5 shows the results of an analysis of first time gate data collected with a handheld EM61 sensor (EM61-HH) on a test stand over various UXO and clutter items in preparation of demonstration at the APG Standardized UXO Test Site. The EM61-HH is a handheld time domain instrument that measures the induced field at time delays of 147, 263, 414 and 613 μsec after the transmit pulse cutoff. In Figure 5 the primary beta value (β_1) for the first time gate is plotted along the horizontal axis. The average of the two secondary betas (β_2 and β_3) for the first time gate is plotted along the vertical axis, and the vertical line stretches between the values of the secondary betas. The beta values for the ordnance are as expected: the larger ordnance items have larger βs, clustered close to a different point for each ordnance type, and the two secondary betas are smaller and equal. The beta values for the clutter are scattered, with secondary beta values usually different from each other.

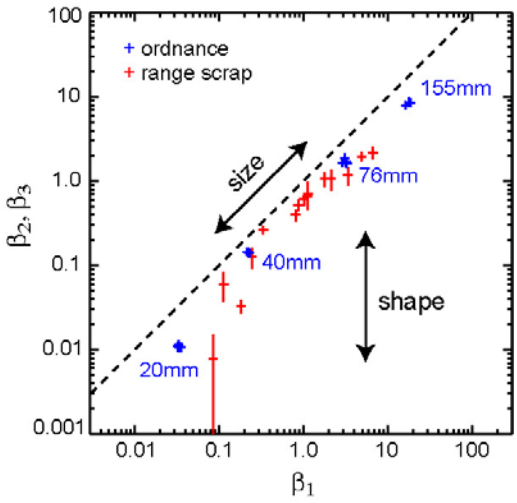

Figure 5 – Beta values for various UXO and clutter items.

Determining the βs from EMI data collected over a buried object is fairly straightforward. Referring back to Figure 4, as the sensor is moved around, data from different locations above the target combine the elements of the polarizability matrix **B** in different ways: the object is excited from different directions and the sensitivity of the receiver to the different response components charnes As it turns out, if data are collected over an area whose dimensions are somewhat larger than the depth of the object, then all of the elements in **B** contribute enough, and in enough different ways to the overall response that the data may be inverted to determine the βs.

If data are collected at N locations ($\mathbf{r}_i$, i=1,2,…,N) over an unknown object, then we have an overdetermined set of N simultaneous equations with nine unknown quantities (three βs, three Euler angles that define the object's orientation, and the XYZ coordinates of the unknown target location $\mathbf{r}_0$):

$$S_i = \mu_0 A I_0 \mathbf{C}_R(\mathbf{r}_0 - \mathbf{r}_i) \cdot \mathbf{C}_T(\mathbf{r}_0 - \mathbf{r}_i)\mathbf{U}\mathbf{B}_0\mathbf{U}^T, \qquad i=1,2,\ldots,N. \tag{7}$$

The equations are solved in a least-squares sense simultaneously for all values of time or frequency. This is accomplished by using a Levenberg-Marquardt gradient search technique to determine the target parameters that minimize the mean squared error between the dipole response model and the measured data. Sensor orientation variations during data collection are accommodated by transforming the target location $\mathbf{r}_0$ and polarizability matrix $\mathbf{B} = \mathbf{U}\mathbf{B}_0\mathbf{U}^T$ into appropriately aligned coordinates at each measurement point.

Figure 6 shows examples of the dipole model fit. In these examples, data were collected using the EM61-HH sensor on a 75 cm square 6x6 rectangular grid. The data shown in Figure 6 are from the earliest time gate. The top pair of plots is for data collected on a test stand, 38 cm above a 25 cm wide by 48 cm long piece of range scrap. The bottom pair is for data collected over a buried 81 mm mortar (depth 50 cm) at the APG Standardized UXO Test Site. On the left are scatter plots of dipole fit signal *vs.* the measured signal. On the right are contour plots of the model fit and the data. The 36 dots show the locations of the measurements. The model fit and the data contours are virtually indistinguishable.

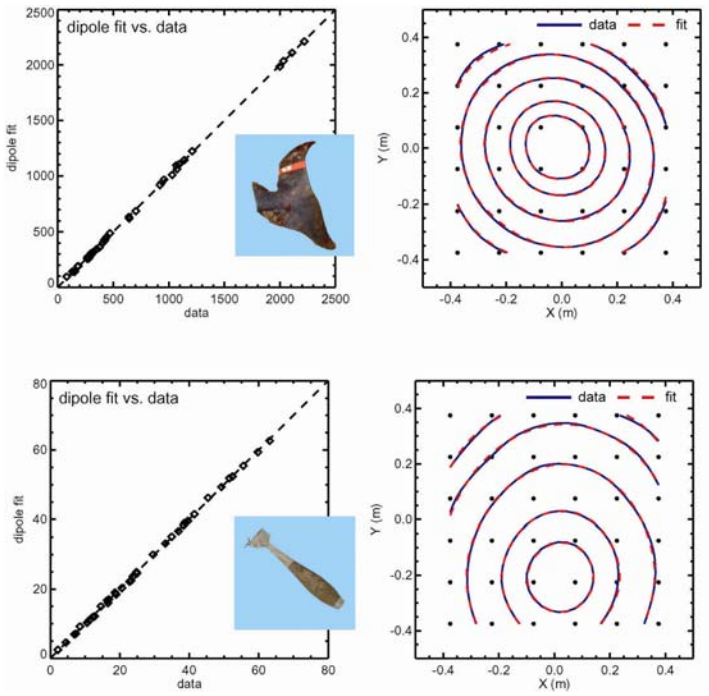

Figure 6 – Examples of dipole model fits to spatially mapped data collected using a Geonics EM61-HH sensor.

Although the signal patterns in Figure 6 appear rather nondescript, they contain enough information to distinguish between the targets. Best fit βs for the range scrap item are $\hat{\beta}$ = 4.32, 3.76 and 2.64, while those for the 81 mm mortar are 2.50, 1.36 and 1.30. The circumflex (^) is used to indicate that these are best fit values for a particular data set. We purposefully cite βs without units. As a practical matter, calibrated, device-independent βs are at best hard to come by. While we may be able to ascertain the actual coil geometry of a sensor, the driving current and the factors that combine to determine the

constant A in equation (2) may be proprietary to the instrument maker. Consequently, although the correct physical dimensions for time domain βs are $[L^3T^{-1}]$, we quote values in arbitrary units that are relevant only to this sensor. In any event, the mortar has one large and two smaller, roughly equal βs. This is appropriate for a cylindrical object. The range scrap has three distinct βs. On this basis, it is easy to decide which object is UXO and which is clutter. This is discrimination on its most basic level, and it does adequate service as a paradigm for the discrimination process in general. More sophisticated schemes incorporate the time or frequency dependence of the βs [10, 26-29], but still must contend with estimating the βs from spatially mapped data.

4. Effects of Noise and Position Errors

We chose the examples shown in Figure 6 because the fits were very good. A useful measure of the goodness of fit is the squared correlation coefficient (ρ^2) between the data and the dipole model fit to the data. We call this the dipole fit quality. In both cases $\rho^2 > 0.9999$. Comparable inversion results can be obtained with the full scale EM61 Mk2 using a grid template. The Mk2 has ½ m by 1 m rectangular coils and measures the induced field at time delays of 216, 366, 660 and 1266 μsec after the transmit pulse cutoff. We used a 6x5 point grid template with dimensions 1 m by 1.6 m. By way of example, using a 60mm mortar target 38 cm below the coils the data are fit very well ($\rho^2 = 0.9996$) using the dipole response model, with $\hat{\beta}$ = 0.196, 0.069, 0.067 for the first time gate.[†]

These examples are for sensors used in what is commonly referred to as a cued identification mode. Target locations have already been determined and perhaps flagged. The sensor (and in this case grid template) is set up over each target location in turn and data are collected. The data are precisely located through the use of the grid template placed over the target. The template is marked with a pattern of perpendicular lines. The line intersections identify the grid points. For the EM61-HH, a sheet of plexiglass marked with crosshairs was attached to the bottom of the sensor head. For the Mk2, crosshair marks were made on the coils. Readings were taken with the sensor crosshairs aligned with the template grid lines, probably to within a few mm. The most successful demonstrations of UXO/clutter discrimination to date have used cued identification with template-gridded data: Geophex GEM-3 at Jefferson Proving Ground [30] and EM61-HH at the Standardized Test Site at Aberdeen Test Center [31]. The approach has also been used successfully at active UXO cleanup sites [32, 33].

As noted in the introduction, several projects underway in SERDP/ESTCP and elsewhere are attempting to develop sensor arrays for cued identification that are configured in such a way that they can simultaneously excite the target from the full complement of directions. Demonstrations of their utility and practicality are underway. For the grid template techniques in use today, an experienced crew can do about 25-40 targets per day. Production rates could be significantly increased if we could reliably use survey data for target classification and discrimination. Depending on the survey platform and whether it is human powered or towed by a vehicle, survey rates can easily exceed 1 hectare per day, and depending on the site there may be many dozens of targets per hectare. Magnetic survey data of sufficient quality to support target characterization is routinely achievable. However, as noted previously, the target information that can be extracted from magnetometer data is of rather limited utility for UXO/clutter discrimination. Obtaining EMI survey data that can be reliably inverted to estimate target βs is much more difficult. Indeed, discrimination performance using the MTADS EM61 array in the field has been uniformly poor relative to expectations based on results of inverting controlled measurements over ordnance and exploded shell fragments [34, 35]. Data collected with the MTADS system is geo-located using multi-antenna differential GPS combined with an inertial measurement unit to track sensor orientation as well as location [36, 37]. The major factors limiting performance in the field are positioning errors and background noise due to small metal fragments which frequently litter ordnance impact areas. Both of these factors can be thought of as contributing noise to the inversion process. If the locations $\mathbf{r}_i$ of the sensor readings S_i used to estimate the target parameters are in error, then the model (2) cannot rightly reproduce the data. And if it can, it will do so using target parameters that are incorrect. Similarly, if the sensor readings include significant contributions from sources other than the target signal, then the dipole model fit will be degraded.

[†] Recall that the βs are instrument specific and have to be re-scaled in order to permit meaningful comparison between sensors.

We have run simulations of the effect that background noise and position errors have on the inversion process. The simulations are based on the EM61 Mk2 data collected over a 60mm mortar. Figure 7 shows the effect of added white Gaussian background noise on dipole fit quality for the grid template configuration described at the beginning of this section. The signal to noise ratio is defined in terms of the peak signal (S_{max}) and the RMS background noise level (σ_N):

$$\mathrm{SNR} = 20\log\left(\frac{S_{max}}{\sigma_N}\right). \tag{8}$$

Statistically speaking, the quantity $1-\rho^2$ is the portion of the signal variance that is not accounted for by the model [38]. This is appropriate if we think in terms of how well the model reproduces the signal at a randomly selected location in the patch of data submitted to the inversion procedure. Hence we expect that $\sqrt{(1-\rho^2)} \propto \sigma_N/S_{max}$. The dashed line in Figure 7 shows the expected relationship between SNR and dipole fit quality. Factor S_0 is 20 log of the proportionality constant, and is equal to about 9.2 dB in this example.

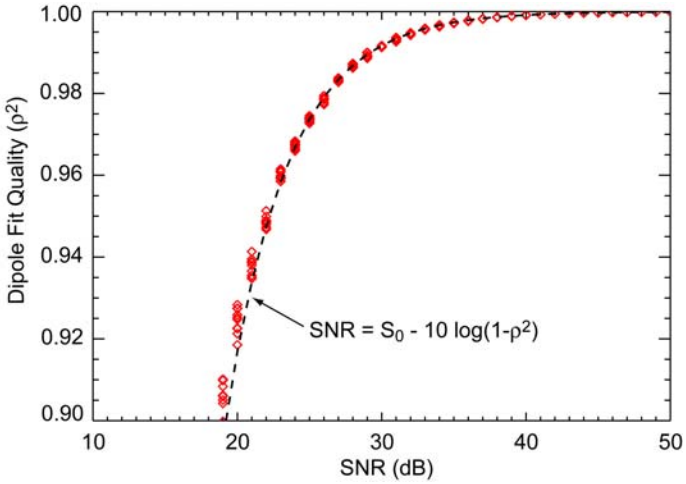

Figure 7 – Dipole fit quality *vs.* target signal to noise ratio from EM61 Mk2 simulations.

Figure 8 shows dipole fit quality *vs.* SNR for an EM61 demonstration at the YPG Standardized UXO Test Site, reproduced from Figure 10 of the MM-0413 Final Report [2]. The red curve gives the expected relationship between ρ^2 and SNR for parameters corresponding to the survey (lane spacing ½ m with sample spacing ~10 cm, resulting in S_0 = 12.2 dB). Although the fit quality appears to be good for high SNR, it is not as good as we would expect. For SNR > 37.4 dB, ρ^2 should exceed 0.997. While two-thirds of the data have SNR > 37.4 dB, only 25% have ρ^2 > 0.997. Something else besides background noise is degrading the quality of the dipole inversion of these data. We suspect that it is geo-location errors.

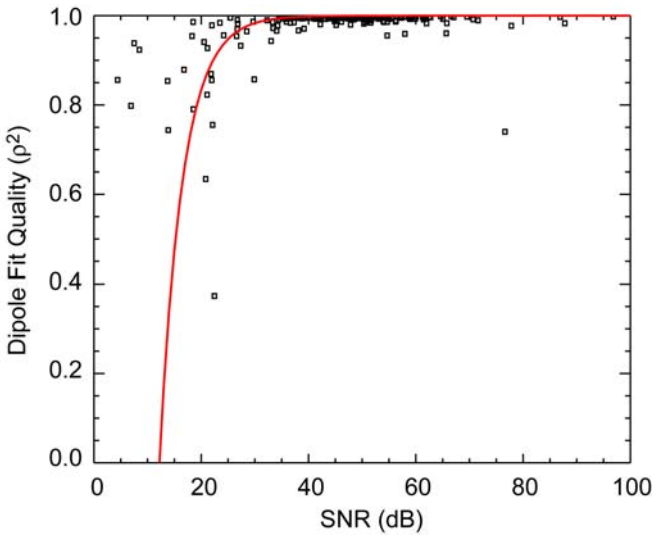

Figure 8 – Dipole fit quality *vs.* SNR for EM61 survey at YPG Standardized UXO Test Site.

Figure 9 shows the effect of position errors on dipole fit quality for the EM61 Mk2 template configuration corresponding to Figure 7. In the simulation, the position errors are uncorrelated, circular Gaussian. The effective noise should be proportional to position error δr, and for this case the dashed line shows the expected relationship between dipole fit quality and position error. Clearly it does not take much geo-location error to have a noticeable effect on dipole fit quality.

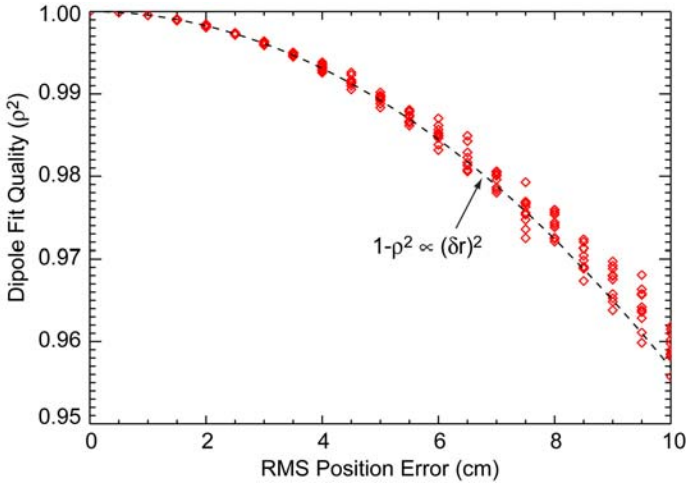

Figure 9 – Dipole fit quality *vs.* position error from EM61 Mk2 simulations.

Since the simultaneous equations (7) are linear in the polarizability elements, errors in estimates of the polarizability matrix will be proportional to the errors in the S_i, with the constant of proportionality determined by details of the coil sensitivity functions $\mathbf{C}_R$ and $\mathbf{C}_T$ [10, 39]. Figure 10 shows the relationship between errors in the polarizabilities (βs) and the dipole fit error $\sqrt{(1-\rho^2)}$. The polarizability (β) error is defined as

$$\beta_{ERR} = \sqrt{\frac{1}{3}\sum_{i=1}^{3}\left(\frac{\hat{\beta}_i - \hat{\beta}_{0,i}}{\hat{\beta}_{0,i}}\right)^2} \qquad (9)$$

where the $\hat{\beta}_i$ are βs calculated using either erroneous locations for the sensor readings or noisy data, and $\hat{\beta}_{0,i}$ are the values of $\hat{\beta}_i$ calculated using the nominal grid positions with no added noise. For small dipole fit errors, the polarizability error scales linearly with fit error, as expected. The β errors are a bit higher for positioning error than for additive noise. This appears to be related to the fact that in the case of position errors, the effective noise is not uniform, but rather varies depending on the signal gradient, while in the case of additive noise, it is uniform. When we run simulations using nonuniform additive noise (σ_N proportional to signal strength), we reproduce the β error levels obtained using position errors. In either case, the errors in our estimates of the polarizabilities start to become unacceptably large for dipole fit errors greater than a few percent, *i.e.* for dipole fit quality (ρ^2) less than about 0.995.

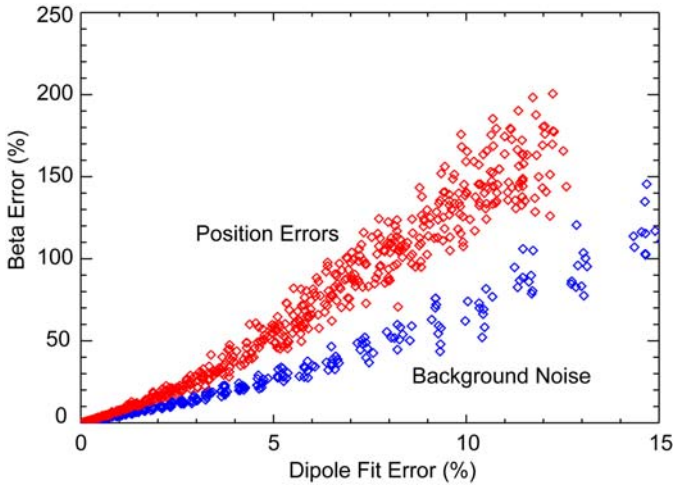

Figure 10 – Polarizability error *vs.* dipole fit error from EM61 Mk2 simulations.

Figure 11 shows simulation results for the dependence of polarizability error on position error. The blue triangles are for the EM61 Mk2 template. The green circles simulate a survey with lane spacing the same as the template ΔX (40 cm), but with ΔY = 10 cm instead of 20 cm, and using 1.6 m of data in the along track (Y) direction instead of 1.0 m. The β errors are reduced by about a factor of 4. Reducing the lane spacing to 10 cm (red diamonds) has only a modest further effect. In the case of the surveys, we need to keep geo-location errors to within 3 or 4 cm RMS in order to maintain β_{ERR} within 15%. This is certainly within the performance specifications of good differential GPS, but can only be achieved at the sensor if the mapping between the GPS antenna and the sensor coils is equally good. Typically, the GPS antenna is mounted some distance above the coils. Since a 2º tilt causes a 3.4 cm offset at the end of a one meter lever, the attitude of the sensor system must be accurately measured and properly synched with the GPS.

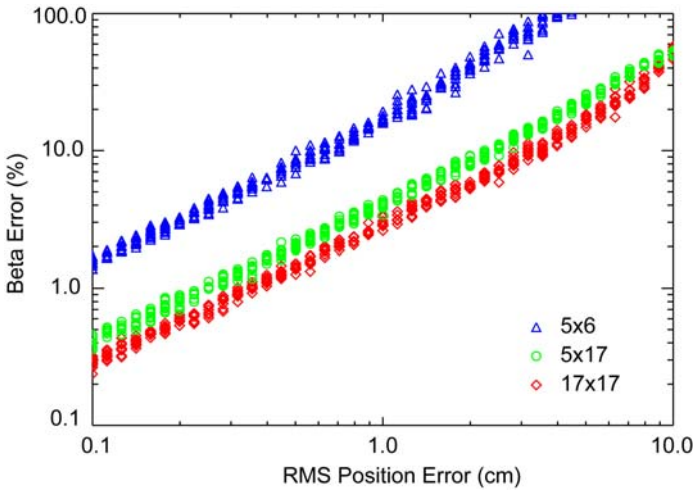

Figure 11 – Beta error *vs.* position error from EM61 Mk2 simulations for three data densities.

5. Conclusion

From our analysis of the effect of positioning errors on the inversion of spatially mapped geophysical data we conclude that centimeter-scale relative accuracy in the recorded positions of sensor readings is required to support reliable target classification and discrimination. We also note that noise levels need to be 30 dB or more less than RMS signal levels in order to realize the performance potential of accurately mapped data. To date, this has only been demonstrated with cued identification systems that use grid templates to accurately position the data readings.

6. References

[1] Teefy, Dennis, "Final Report for the Evaluation of Unexploded Ordnance (UXO) Detection Technology at the Standardized UXO Test Sites Aberdeen and Yuma Proving Grounds," US Army Aberdeen Test Center Report ATC-9379, November 2007.

[2] "Standardized Analysis for UXO Demonstration Sites: Final Report," ESTCP Project MM-0413 Final Report, April 2008.

[3] Barrow, B., and H. Nelson, "Collection and Analysis of Multi-Sensor Ordnance Signatures with MTADS," *J. Environmental and Engineering Geophysics*, 3(2), pp. 71-79, June 1998.

[4] Nelson, H., T. Altshuler, E. Rosen, J. McDonald, B. Barrow and N. Khadr, "Magnetic Modeling of UXO and UXO-like Targets and Comparison with Signatures Measured by MTADS," Proceedings of the UXO Forum, Anaheim, pp. 282-291, May 1998.

[5] Billings, S., L. Pasion and D. Oldenburg, "UXO Discrimination and Identification Using Magnetometry," Symposium on the Application of Geophysics to Environmental and Engineering Problems, Las Vegas, February 2002.

[6] Billings, S., L. Pasion and D. Oldenburg, "Inversion of Magnetics for UXO Discrimination and Identification," UXO/Countermine Forum, Orlando, September 2002.

[7] Das, Y., J. McFee, J. Toews and G. Stuart, "Analysis of an Electromagnetic Induction Detector for Real-Time Location of Buried Objects," *IEEE Transactions on Geoscience and Remote Sensing*, 28(3), pp. 278-288, May 1990.

[8] McNeill, J. and M. Bosnar, "Application of Time Domain Electromagnetic Techniques to UXO Detection," Proceedings of the UXO Forum, Williamsburg, pp. 34-42, March 1996.

[9] Bell, T., B. Barrow and J. Miller, "Subsurface Discrimination Uusing Electromagnetic Induction Sensors," *IEEE Transactions on Geoscience and Remote Sensing*, 39(6), pp. 1286-1293, June 2001.

[10] Pasion, L. and D. Oldenburg, "A Discrimination Algorithm for UXO Using Time Domain Electromagnetics," *J. Environmental and Engineering Geophysics*, 6(2), pp. 91-102, June 2001.

[11] Norton, S. and I. J. Won, "Identification of Buried Unexploded Ordnance from Broadband Electromagnetic Induction Data," *IEEE Transactions on Geoscience and Remote Sensing*, 39(10), pp. 2253-2261, October 2001.

[12] Barrow, B. and H. Nelson, "Model-Based Characterization of Electromagnetic Induction Signatures Obtained with the MTADS Electromagnetic Array," *IEEE Transactions on Geoscience and Remote Sensing*, 39(6), pp. 1279-1285, June 2001.

[13] Grimm, R., "Triaxial Modeling and Target Classification of Multichannel, Multicomponent EM Data for UXO discrimination," *J. Environmental and Engineering Geophysics*, 8(4), pp. 239-250, December 2003.

[14] Young, R. "Geophysical Characterization at OE Sites," UXO Forum, Anaheim, May 1998.

[15] McDonald, J., "Detailed Comparison of a 'Mag and Flag' UXO Clearance with Geo-Referenced Digital Geophysics Using Multi-Sensor Towed Arrays," UXO/Countermine Forum, Anaheim, May 2000.

[16] Fairbanks, J., "Baseline Performance of Traditional and Emerging UXO Detection Technologies," UXO/Countermine Forum, St. Louis, March 2004.

[17] Nelson, H. and J. McDonald, "Multisensor Towed Array Detection System for UXO Detection," *IEEE Transactions on Geoscience and Remote Sensing*, 39(6), pp. 1139-1145, June 2001.

[18] Altshuler, T. "Shape and Orientation Effects on Magnetic Signature Prediction for Unexploded Ordnance," Proceedings of the UXO Forum, Williamsburg, pp.282-291, March 1996.

[19] Billings, S., J. Stanley and C. Youmans," Magnetic Discrimination that will Satisfy Regulators?" UXO/Countermine Forum, Orlando, September 2002.

[20] Landau, L. and E. Lifshitz, *Electrodynamics of Continuous Media*, Pergamon Press, 1960.

[21] Baum, C. (ed.), *Detection and Identification of Visually Obscured Targets*, Taylor and Francis, 1999.
[22] "Handheld UXO Sensor Improvements to Facilitate UXO/Clutter Discrimination," SERDP Project MM-1381 Final Report, October 2007.
[23] Goldstein, H., *Classical Mechanics*, 2nd ed., Addison-Wesley, 1980.
[24] Miller, J., T. Bell, J. Soukup and D. Keiswetter, "Simple Phenomenological Models for Wideband Frequency-Domain Electromagnetic Induction," *IEEE Transactions on Geoscience and Remote Sensing*, 39(6), pp. 1294-1298, June 2001.
[25] Smith, J. T., H. F. Morrison and A. Becker, "Parametric Forms and the Inductive Response of a Permeable Conducting Sphere," *J. Environmental and Engineering Geophysics*, 9(4), pp. 213-216, December 2004.
[26] Barrow, B., N. Khadr, H. Nelson and D. Steinhurst, "Results from a Towed Array of Multiple Frequency EMI Sensors," UXO/Countermine Forum, St. Louis, March 2004.
[27] Barrow, B., N. Khadr, J. Miller and H. Nelson," An Empirically Based Elliposoidal Model for Multiple Frequency EMI Signatures from UXO, "Symposium on the Applications of Geophysics to Engineering and Environmental Problems, Atlanta, April 2005.
[28] MacInnes, S., D. Snyder and K. Zonge, "Physics-Based Characterization of UXO from Multi-Component TEM Data," UXO/Countermine Forum, Orlando, September 2002.
[29] Snyder, D., S. MacInnes, J. Hare, R. Grimm, M.Poulton and A. Szidarovsky," The Value of Multi-Component TEM Data for the Estimation of UXO Target Parameters," Symposium on the Applications of Geophysics to Engineering and Environmental Problems, Colorado Springs, February 2004.
[30] Robitaille, G., J. Adams, C. O'Donnell and P. Burr, "Jefferson Proving Ground Technology Demonstration Program Summary," Army Environmental Center report SFIM-AEC-ET-TR-99030, May 1999.
[31] ESTCP Project 200108 Cost and Performance Report, "Handheld Sensor for UXO Discrimination," October 2004.
[32] Ambrose, B., T. Bell and T. Furuya, "UXO Clearance at the Lake Success Redevelopment Project," UXO/Countermine Forum, Saint Louis, March 2004.
[33] Foley, J., M. Miele, R. Mehl, J. Dolynchuk, J. Hodgson and J. Swanson, "Procedures for Applying UXO Discrimination Technology at the Former Lowry Bombing and Gunnery Range," UXO/Countermine Forum, Saint Louis, March 2004.
[34] Barrow, B. and H. Nelson, "Effects of Positioning Error on Inverting EMI Data for UXO Discrimination Using the MTADS Platform," UXO/Countermine Forum, New Orleans, April 2001.
[35] Barrow, B. and H. Nelson, "EMI Signatures from Large Projectiles and Exploded Projectile Fragments on a Seeded Live Site," UXO/Countermine Forum, Orlando, September 2002.
[36] Steinhurst, D., N. Khadr and B. Barrow, "Characterization of Dynamic Platform Motion under Real-World Conditions," UXO/Countermine Forum, Saint Louis, March 2004.
[37] Steinhurst, D., N. Khadr, B. Barrow and H. Nelson, "Moving Platform Orientation for an Unexploded Ordnance Discrimination System," *GPS World*, 16(5), pp. 28-34, May 2005.
[38] Cramer, H., *Mathematical Methods of Statistics*, Princeton University Press, 1946.
[39] Smith, J. T. and H. F. Morrison, "Estimating Equivalent Dipole Polarizabilities for the Inductive Response of Isolated Conductive Bodies," *IEEE Transactions on Geoscience and Remote Sensing*, 42(6), pp. 1208-1214, June 2004.